UNSTEADY REYNOLDS AVERAGED NAVIER-STOKES (URANS) MODELLING OF TURBULENT FLOW IN A TWIN RECTANGULAR SUB-CHANNEL GEOMETRY

G. Arvanitis[1,2], D. Home[1,2], M.F. Lightstone[1] and M.S. Hamed[1,2]
[1] Department of Mechanical Engineering, [2] Thermal Processing Laboratory (TPL),
McMaster University, Hamilton, Ontario, Canada

Abstract

This paper presents the results of a numerical research that is carried out to predict the turbulence structure in compound rectangular channels using an Unsteady Reynolds Averaged Navier Stokes (URANS) based turbulence model. The studied geometry is a twin rectangular sub-channel. The simulations are performed for two different mesh structures. The model predicts the expected flow pulsations at the gap and the results have clear periodicity and symmetry. In the current phase of this research, studies are performed to accurately predict the characteristics of the flow structures.

1. Introduction

CANDU reactor cores contain cylindrical rod bundle geometries, where coolant flows axially past the rods. An understanding of the behaviour of the fluid flow under normal or abnormal conditions is very important, in order to accurately predict the fuel rod temperatures and ultimately improve the design of the reactor cores. The main interest of the current research is in the fluid flow at the gap regions which connect adjacent sub-channels since flow across the gap aids in fluid mixing and in homogenizing the fluid temperatures across the rod bundles. During the last forty years there has been an extensive research, trying to understand the mechanism that causes these high mixing rates. In the early 1970s, the main trend was to attribute this special mixing process to secondary flows. However, experimental research has indicated that this is not the case. Experiments have shown that large-scale flow pulsations are mainly responsible for the mixing between sub-channels [1,2,3].

It has been demonstrated that the same flow pulsation phenomena also occur in rectangular compound channels [4]. Meyer and Rehme performed a very detailed experimental study in 1994 [4]. Their experiments showed that a quasi periodic large scale turbulence structure exists in any longitudinal slot or groove in a wall or a connecting gap between two flow channels, provided that the gap's depth is more than approximately twice its width. The above-mentioned similarity between fluid flow in rod bundle geometries and fluid flow in compound rectangular geometries is the basic reason of choosing the latter geometries in the present work. Another reason for this choice is that the experimental investigation of Meyer and Rehme provides enough flexibility to perform a parametric study. So, in the present work, simulations are carried out with the goal of predicting the turbulence structure in compound rectangular channels as reported in the experiment. Previous attempts to model inter-sub-channel thermal mixing using standard turbulence models have had mixed success. Steady state predictions significantly under predict the mixing since the flow pulsation phenomenon, which is inherently unsteady, is not captured. Previous predictions, using an unsteady Reynolds Averaged Navier Stokes (URANS) model, of isothermal flow in channel containing a single rod and of isothermal flow in rod bundle geometries have shown that the coherent structures in the region between the rod and the wall can be predicted [5,6,7,8]. In the present work the URANS model of Spalart Allmaras (SA) is applied [9]. The SA model was calibrated for aerodynamic flows and is also able to accurately predict vortex shedding. The work, presented in this paper, is part of a broader goal to examine the effect of large scale flow pulsation phenomena on the structure of turbulence, identify the coherent structures using the structure identification techniques and provide a physical model for the origin of the large scale structures in twin sub-channel geometries.

2. Computational procedure

In this section, the details of the simulations' set up are presented. The simulations were carried out using the commercial code ANSYS CFX-11.0. This code uses a finite volume discretization with a fully implicit time advancement scheme. A second order backward Euler time discretization scheme is applied while advection is approximated using an upwind scheme**.**

2.1 Model

As mentioned in the introduction, the turbulence model used is the Spalart – Allmaras (SA) model [9]. This is a one-transport equation model, which solves for the turbulent eddy viscosity (v_t):

$$\frac{\partial \rho \tilde{\nu}}{\partial t} + \nabla \cdot \rho \vec{U} \tilde{\nu} = c_{b1} \rho \tilde{S} - c_{w1} f_w \rho \left(\frac{\tilde{\nu}}{d} \right)^2 + \frac{\rho}{\sigma} \left[\nabla \cdot (\nu + \tilde{\nu}) \nabla \tilde{\nu} + c_{b2} |\nabla \tilde{\nu}|^2 \right] \quad (1)$$

$\tilde{\nu}$ is defined in such a way that it is equal to v_t everywhere, except in the viscous region, for which: $\chi \equiv \tilde{\nu}/\nu$. v is the kinematic viscosity. The eddy viscosity in the Reynolds stresses is: $\nu_t = \frac{\mu_t}{\rho} = \tilde{\nu} f_{v1}$, where: μ_t is the turbulent dynamic viscosity, ρ is the density and f_{v1} is a function, borrowed from Mellor & Herring [10]. $\vec{U}$ is the velocity, σ is a turbulent Prandtl number and c_{b1}, c_{b2} and c_{w1} are constants of the model. The subscripts b and w stand for basic and wall respectively. f_w is a non dimensional function. In the R.H.S of equation (1) the first term represents the production of the turbulent eddy viscosity. In this term $\tilde{S}$ is a modified velocity gradient norm. The second term in the R.H.S of equation (1) represents the destruction of the turbulent eddy viscosity and the third term represents the diffusion of it.

The idea for the SA model was initiated from Baldwin-Barth's model [11]. The fundamental difference of the SA model compared to the Baldwin-Barth's model is based on the idea that generating a one-equation model as a simplified version of the k-ε model is not optimal [9]. What Spalart and Allmaras did was to generate 'from scratch' all the terms in the transport equation for the turbulent eddy viscosity. So, what they basically did in their original paper was to present four nested versions of the model from the simplest, applicable to free shear flows to the most complete, applicable to viscous flows past solid bodies and with laminar regions [9].

The SA model is a very robust, compatible with various grid structures model, which has already been tested successfully in many different cases with both separated and unseparated boundary layer flows and with various degrees of complexity. Also, it is an inherently unsteady model. Furthermore, the SA model was calibrated for aerodynamic flows and it was used successfully in vortex shedding flows and in general in flows where there is formation of vortex structures. The above reasons provide justification for using this model in the present study, since it has been experimentally observed that a street of counter rotating pairs of vortices in an alternating pattern is formed at the edges of the gap region. Moreover, its computational cost is low compared to other RANS models since it is a one-equation model.

2.2 Geometry

In the current phase of research, the selected geometry is the so-called 'case No.9' of Meyer and Rehme's test cases [4]. Specifically, the cross section of this geometry is shown in Figure 1. In Figure 1 the system of reference can also be seen, together with the respective velocity symbols. The stream-wise direction is in the x-axis, the span-wise direction is in the z-axis and the wall normal direction is in the y-axis. The flow is from the page to the reader. Following Meyer and Rehme's notation, the height of the sub-channels, a, is 180 mm, the height of the gap, g, is 10 mm and the width of the gap, d, is 76.96 mm. The width of the left channel, b_1, is 136.4 mm and the width of the right channel, b_2, is 136.2 mm. The length of the channel used in the experiments was 7,000 mm. A shorter length of L = 730 mm was used in the simulations together with periodic boundary conditions, imposed in the inlet – outlet surfaces. The specific value of L was selected in order to capture three vortex structures in this length of the channel.

2.3 Boundary conditions

As stated before, to ensure independence from the entrance conditions and also to ensure a fully developed flow without having to use a too long channel, periodic boundary conditions are applied in the stream-wise direction. In all the other surfaces of the channel the no slip wall boundary conditions are applied. The mass flow rate, $\dot{m}$, was given as a boundary condition. This mass flow rate corresponds to a Reynolds number of 2.15 x 10^3, based on the bulk velocity, U_b, and the hydraulic diameter, D_h, of the channel.

2.4 Mesh design

Two different grid structures have been used. In the first case (Case 1), the total number of nodes is 633,850. The meshing law is uniform mesh all over the computational domain. In the stream-wise direction (x-direction in Figure 1) there are 50 nodes. In the wall normal direction (y-direction in Figure 1) the total number of nodes is 145, whereas the number of nodes at the gap is 9. In the span-wise direction (z-direction in Figure 1) the total number of nodes is 111, whereas at the gap region there are 25 nodes. The grid structure for the second case (Case 2) is similar to Case 1 except that the number of nodes in the span-wise direction is doubled. Specifically, the total number of nodes in the span-wise direction is 222, whereas at the gap region the number of the span-wise nodes is 50. The total number of nodes in the domain for Case 2 is 1,268,600.

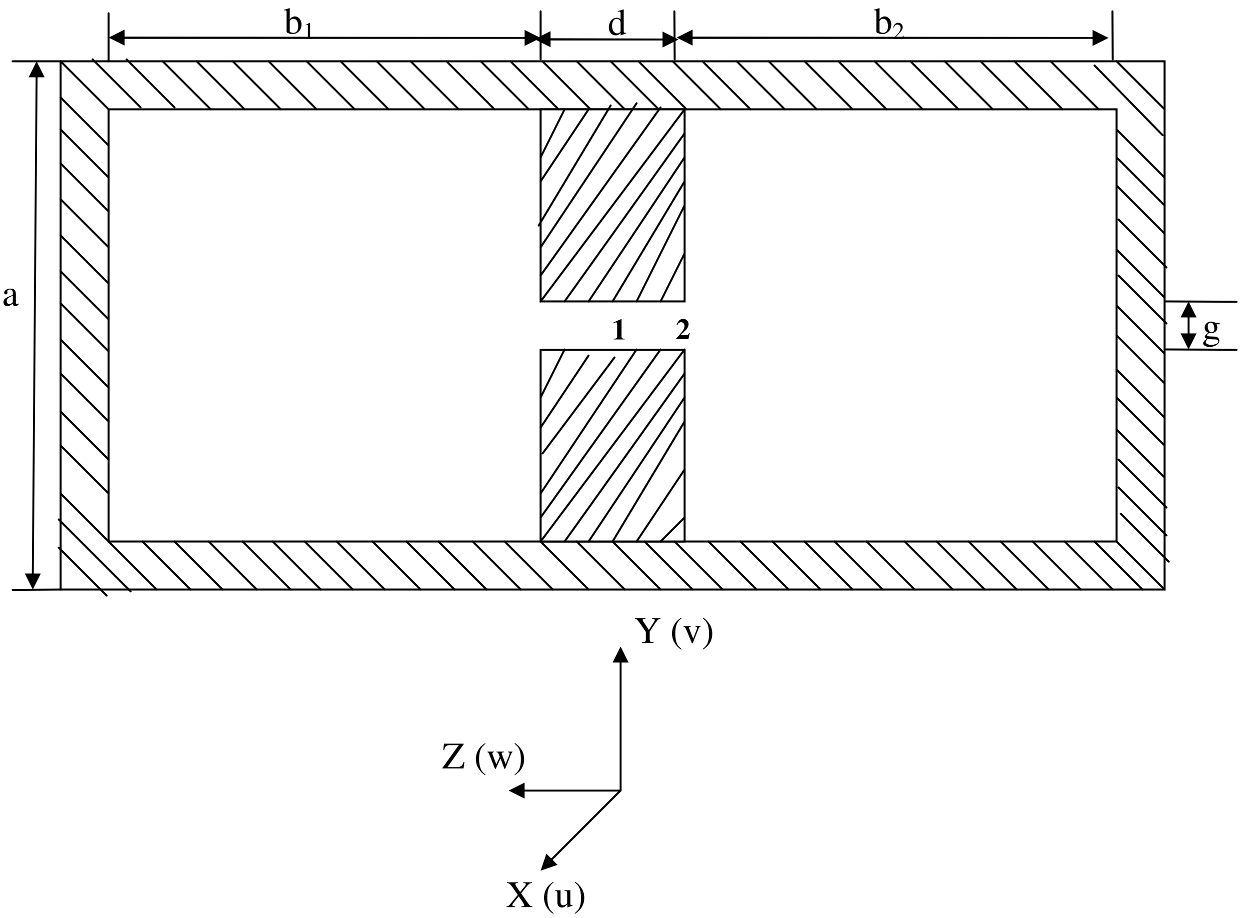

Figure 1 Cross-section and the coordinate axis of the twin rectangular sub-channel geometry.

2.5 Initialisation

An initial profile for the axial velocity is used. This profile was obtained from a steady SST run. The time step is set to 10^{-4} sec. This way based on the bulk velocity and the length of the channel, a particle of fluid travels throughout the domain in about 0.0345 seconds or in 345 time steps. The selected time step is sufficiently short to capture the large-scale coherent structures and it was based on the frequency of these structures, reported in the experiments [4]. As an implicit code, ANSYS CFX-11.0 does not require the Courant number to be small for stability. However, with the current settings, the Courant number is of the order of one. The simulations ran for sufficiently long time in order to obtain a statistically stationary flow field, independent of the initial conditions for the axial velocity. The averaging process starts after 5,000 time steps and it takes place over the next 5,000 time steps. This yields a total simulation time of one second.

3. Results and discussion

In this section part of the results of the simulations are presented followed by a discussion. Specifically, some of the results presented from now on refer to the two points, seen in Figure 1. Point 1 is at the gap centre and point 2 is at the gap edge.

3.1 Velocity plots

The normalized time averaged axial velocity contour for Case 1 is shown in Figure 2. The bulk velocity, $U_b = 21.5$ m/s, is used for the normalization of the axial velocity. There is a clear symmetry with respect to the axis of symmetry through the gap. This contour shows the typical bulging at the corners of the two connected channels, which is attributed to the formation of secondary flows. Right at the gap corners there is a bulging of the contour from the gap edges towards the two sub-channels. This phenomenon must be attributed to the cross flow at the gap. The same qualitative observations were made in the experiments [4]. Furthermore, the velocity magnitudes are also similar to the experimental results. However a slight difference in the shape of the lines of the velocity contour was seen.

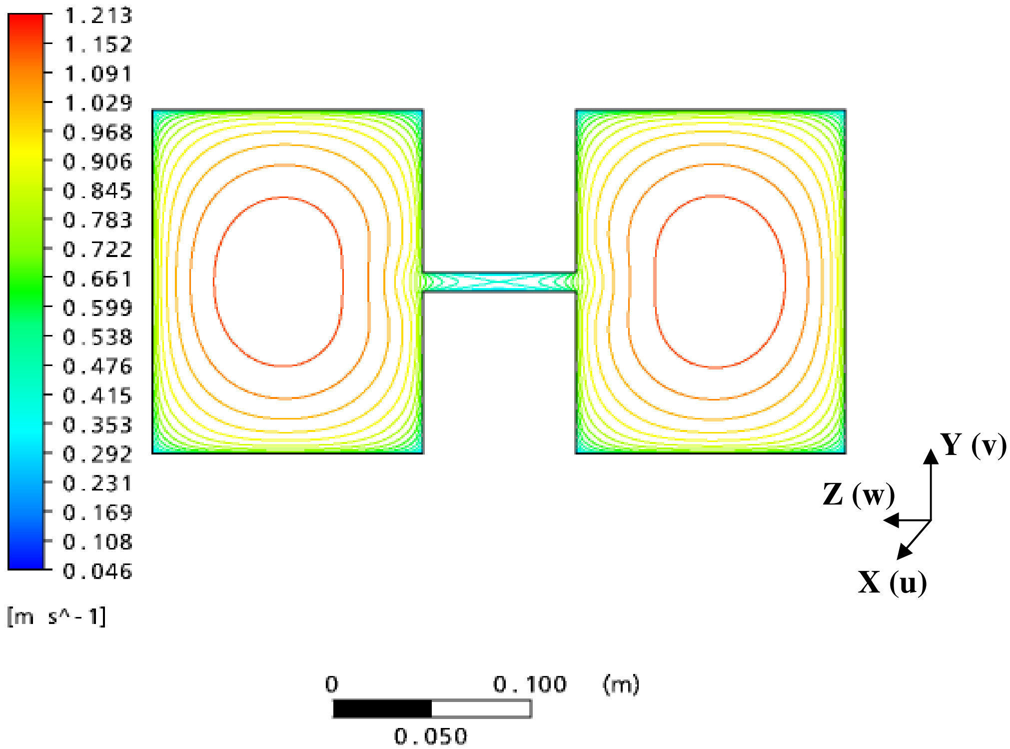

Figure 2 Normalized Axial (u) Velocity (Case 1)

The span-wise velocity contour at the symmetry plane through the gap for Case 2 is shown in Figure 3. The gap region is clearly noted by the two black lines at about the centre of the channel. The figure clearly shows an alternate pattern of large-scale flow structures. As it can be seen from the legend on the left of Figure 3 there is an excellent symmetry in the predicted values of the span-wise velocity, which were also observed in the experimental results. In addition, the magnitude of these velocity values is very close to the respective experimental values.

Compared to Case 2, Case 1 slightly under predicts the span-wise velocity. This indicates that additional grid sensitivity tests should be performed. However, the frequency and the wavelength of the flow pulsations in both of the two computational cases are the same. As shown in Table 1, the computed frequency is under predicted by almost a factor of two compared to the experiment [4] and the wavelength is over predicted compared to its experimental value [4]. In Figure 4 the velocity vector at the symmetry plane through the gap is shown. Based on the contour plot in Figure 3, this wiggly pattern of the velocity in Figure 4 was expected.

Figures 3 and 4 show that the fluid is being pushed in the span-wise direction in an alternate sequence through the gap. The high velocity gradients at the edges of the gap, where two shear layers meet, is responsible for the formation of the vortex structures. As can be seen from Figure 3, two consecutive vortices rotate in opposite directions. The large-scale flow structures are driven by the high velocities in the two sub-channels.

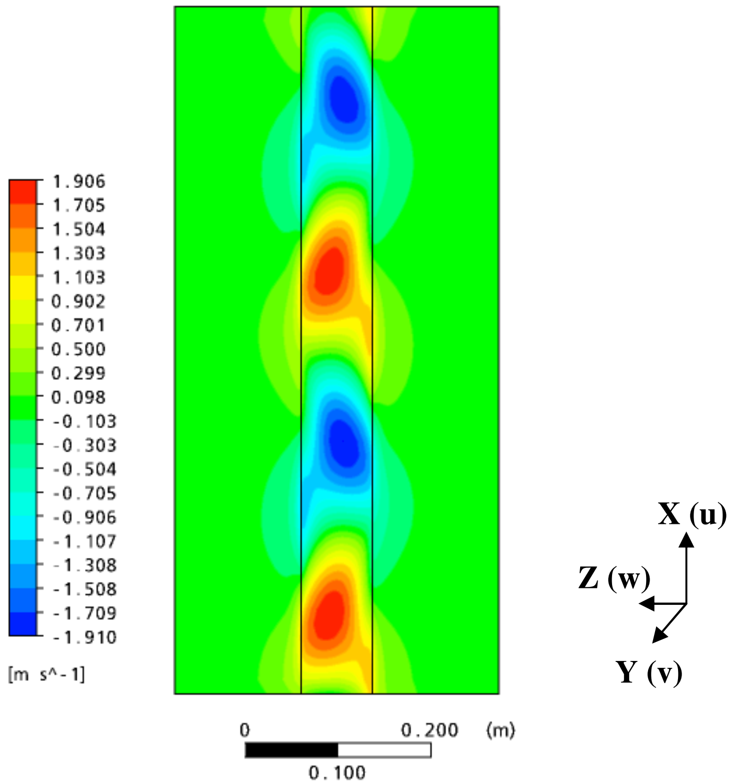

Figure 3 Span-wise velocity (*w*) contour at the symmetry plane through the gap (Case 2)

	Frequency (Hz)	**Wavelength (m)**
Cases 1 and 2	32.26	0.36
Experiment [4]	68	0.2

Table 1 Frequency and wavelength comparison

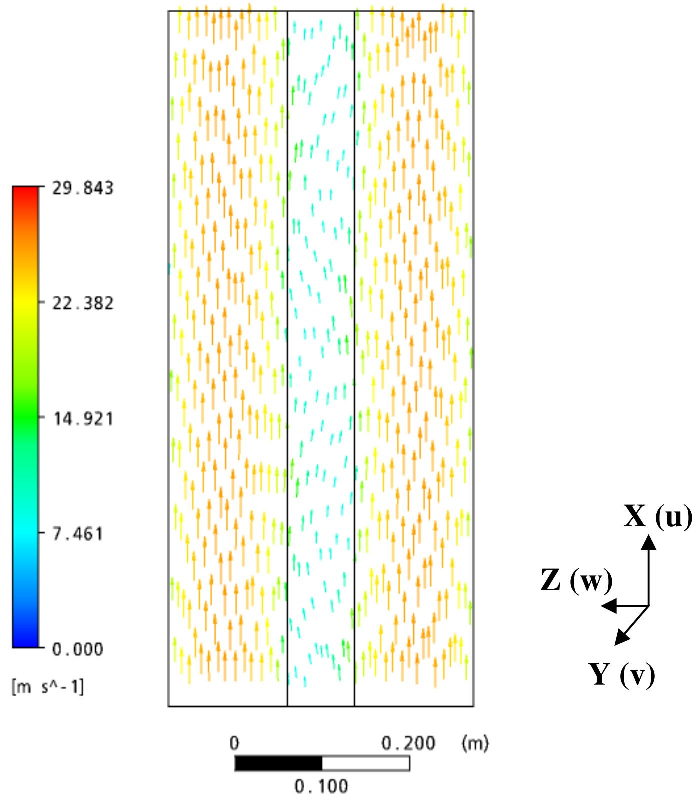

Figure 4 Velocity vector plot at the symmetry plane through the gap (Case 2)

3.3 Turbulent axial intensity and turbulent kinetic energy contours

Figures 5 and 6 present contour plots of the normalized axial turbulent fluctuation, *u'*, and the normalized turbulent kinetic energy, *k*, respectively, for Case 2. The average friction velocity, u^*, is used for the normalization of both variables. The turbulent kinetic energy is given by:

$$k = \frac{1}{2}\left(\overline{u'^2} + \overline{v'^2} + \overline{w'^2}\right) \tag{2}$$

In equation (2), *u'*, *v'*, and *w'* are the turbulent intensities in the axial (X), transverse (Y), and span-wise (Z) directions, respectively. It can be observed from Figure 5 that very high axial intensities are present at the edges of the gap, as it was also observed in the experiments [4]. The peak value of the axial intensity ($u' = 3.4$) matches the respective experimental value.

The normalized turbulent kinetic energy contour, *k*, shown in Figure 6, has been normalized using the squared average friction velocity, u^*. Figure 6 shows a good symmetrical distribution of *k* around the symmetry line through the gap. The *k* contours have two peaks at the two edges of the gap. This was expected from the axial intensity, *u'*, contour, since *k* should follow. This was expected from the axial intensity, *u'*, contour, since *k* should follow the same trend as *u'*. The peak value is under predicted compared to the experiment [4]. However, the peak value in Case 2 is higher than the peak value in Case 1. The distributions of the turbulent intensities in both cases follow the same trends at the gap region reported in the experiments [4]. However, the peak values are under predicted compared to the experimental peak values.

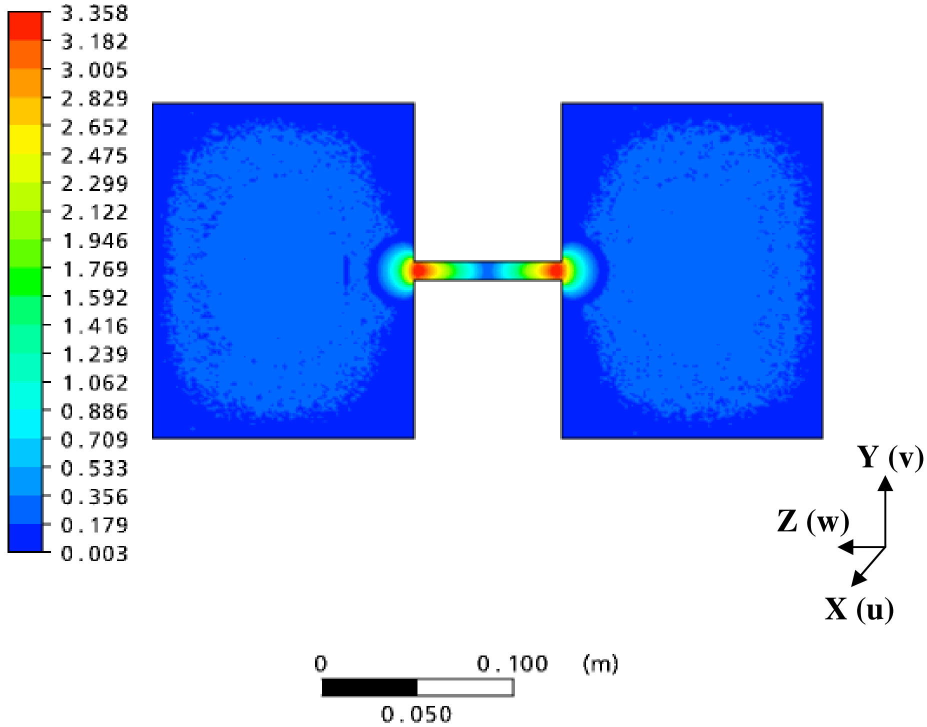

Figure 5 Normalized turbulent axial intensity (*u'*) contour (Case 2)

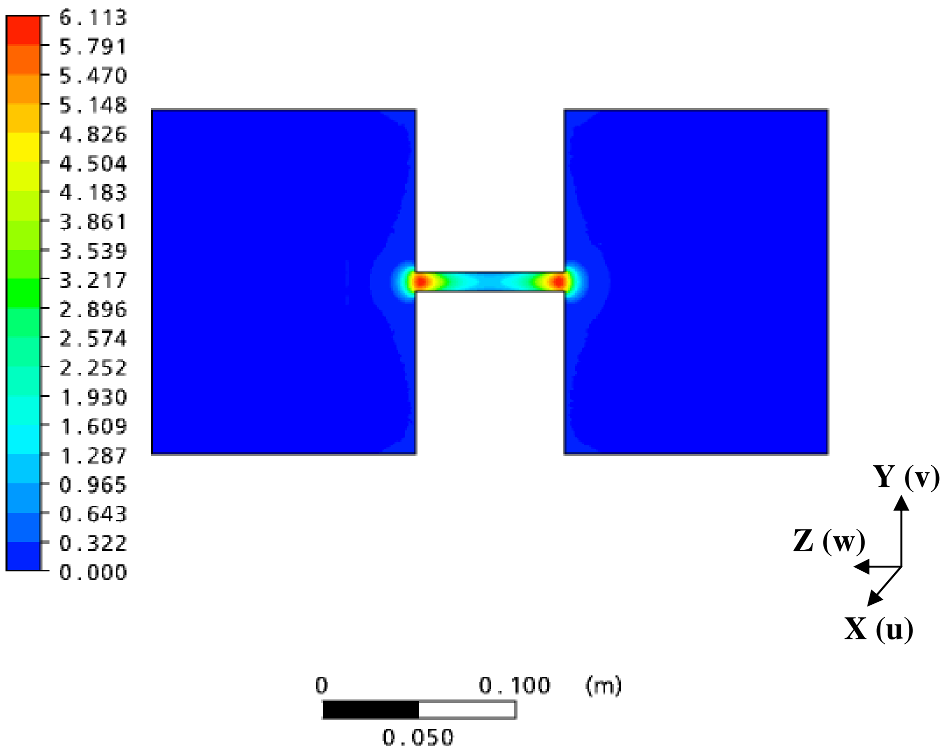

Figure 6 Normalized turbulent kinetic energy (*k*) contour (Case 2)

3.4 Velocity time traces

In the following figures the time variation of the span-wise velocity at the gap centre and at the gap edge (Points 1 and 2 in Figure 1) in Case 2 are presented. Clear symmetry and periodicity can be observed in these results. However, in the experiments [4] there was not a clear symmetry and the results showed a quasi-periodicity. The resulting frequencies of these time traces are tabulated in Table 1.

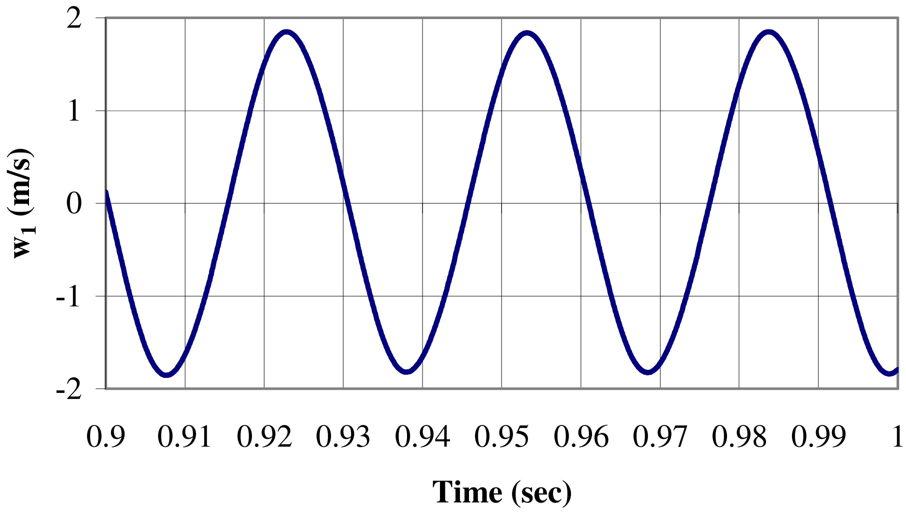

Figure 7 Time trace of the span-wise velocity at the gap centre (w_1) (Case 2)

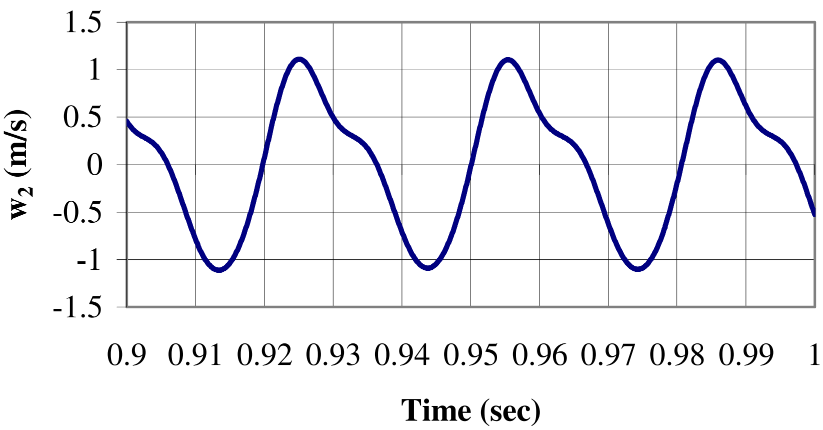

Figure 8 Time trace of the span-wise velocity at the gap edge (w_2) (Case 2)

4. Conclusion

The SA model was successfully used in predicting large-scale flow structures at the gap. This was expected, since the SA model is calibrated for flows with formation of vortices. In addition, this paper shows that a URANS approach can have good qualitative agreement with experiments, where formation of large-scale flow structures is observed [6,7].

There is a good qualitative agreement of the results with the general physical phenomenon, as described by Meyer and Rehme [4]. Clear periodicity and symmetry is identified in the results of the simulations. However, the model under predicts the frequency of the flow structures by almost a factor of two. Furthermore, the predicted wavelength of the vortices is higher than the experimentally observed wavelength [4]. Nonetheless, the magnitudes of the fluid velocities are well predicted. It is worth noting that the results for Case 2 are closer to the experimental measurements. This suggests that an optimization of the number of grid points in the span-wise direction should be made. Specifically, the number of nodes in the span-wise direction should be higher than what has been used for Case 1, in order to obtain quantitatively closer results to the experiment. On the other hand, the number of nodes in the span-wise direction should be less than what has been used in Case 2, because the computational cost in this case is higher than what is expected when a URANS simulation is used, where sufficiently good results are sought with a relatively less computational time.

More work has to be done to assess the grid independence of the model, by also testing the effect of changing the number of nodes in all the three directions. Moreover, the dependence of the results on the Reynolds number must also be assessed. The sensitivity of the SA model can also be tested by adjusting some values, available in the model's version in ANSYS CFX-11.0. Finally, part of this general task is to elaborate on the physical mechanism behind the formation of the large-scale flow pulsations and suggest a flow model to explain the studied phenomenon.

5. Acknowledgments

The funding and support of Natural Sciences and Engineering Research Council of Canada (NSERC) and University Network of Excellence in Nuclear Engineering (UNENE) is greatly appreciated.

References

[1] Guellouz M. S., Tavoularis S., "The structure of turbulent flow in a rectangular channel containing a cylindrical rod – Part1: Reynolds-averaged measurements", *Experimental Thermal and Fluid Science*, Vol. 23, 2000, pp.59-73. – Part2: bPhase-averaged measurements, *Experimental Thermal and Fluid Science*, Vol. 23, 2000, pp.75-91

[2] Rowe, D. S., Johnson, B. M., Knudsen, J.G., "Implications concerning rod bundle crossflow mixing based on measurements of turbulent flow structure", *International Journal of Heat and Mass Transfer*, Vol. 17, 1974, pp.407-419

[3] Möller, S. V., "Single phase turbulent mixing in rod bundles", *Experimental Thermal and Fluid Science*, Vol. 5, 1992, pp.26-33

[4] Meyer L., Rehme K., "Large scale turbulence phenomena in compound rectangular channels", *Experimental Thermal and Fluid Science*, Vol. 8, 1994, pp.286-304

[5] Tavoularis S., Madrane, A., Vaillancourt, R., "Numerical simulation of coherent structures in axial flows through a rectangular channel containing a cylindrical rod", *10th Annual Conference of the CFD Society of Canada*, 2002

[6] Merzari E., Ninokata H., Baglietto E., "Unsteady Reynolds averaged Navier-Stokes simulation for an accurate prediction of the flow inside tight rod bundles", *12th International Topical Meeting on Nuclear Reactor Thermal Hydraulics (NURETH-12)*, 2007

[7] Chang D., Tavoularis S., "Numerical simulation of turbulent flow in a 37-rod bundle", *Nuclear Engineering and Design*, Vol. 237, 2007, pp. 575-590

[8] Chang D., Tavoularis S., "Identification of coherent structures in axial flow in a rectangular channel containing a rod", *12th Annual Conference of the CFD Society of Canada*, 2004

[9] Spalart P. R., Allmaras S. R., "A one-equation turbulence model for aerodynamic flows", *30th Aerospace Sciences Meeting & Exhibit*, January 6-9, 1992, Reno, NV

[10] Mellor, G. L., Herring, H. J., "Two methods of calculating turbulent boundary layer behaviour based on numerical solutions of the equations of motion", *Proc. Conf. Turb. Boundary Layer Pred.*, Stanford, 1968

[11] Baldwin, B. S., Barth, T. J., "A one-equation turbulence transport model for high Reynolds number wall-bounded flows", AIAA-91-0610